Probing intermolecular interactions in a diethylcarbamazine citrate salt by fast MAS ^{1}H solid-state NMR spectroscopy and GIPAW calculations

Tiago Venâncio [a,d,], Lyege Magalhaes Oliveira [a], Javier Ellena [b], Nubia Boechat [c], Steven P. Brown [d]*

[a] *Departamento de Química, Universidade Federal de São Carlos, Rodovia Washington Luis, km 235, São Carlos, SP, 13565-905, Brazil.*

[b] *Instituto de Física de São Carlos, Universidade de São Paulo, Av. Trabalhador são-carlense, 400, São Carlos, SP, 13566-590, Brazil.*

[c] *Fundação Oswaldo Cruz - FioCruz, Instituto de Tecnologia em Fármacos-FarManguinhos, Rua Sizenando Nabuco 100, Rio de Janeiro, RJ, 21041-250, Brazil.*

[d] *Department of Physics, University of Warwick, Coventry, CV4 7AL, UK*

Abstract

Fast magic-angle spinning (MAS) NMR is used to probe intermolecular interactions in a diethylcarbamazine salt, that is widely used as a treatment against adult worms of *Wuchereria bancrofti* which cause a common disease in tropical countries named filariasis. Specifically, a dihydrogen citrate salt that has improved thermal stability and solubility as compared to the free form is studied. One-dimensional ^{1}H, ^{13}C and ^{15}N and two-dimensional ^{1}H-^{13}C and ^{14}N-^{1}H heteronuclear correlation NMR experiments under moderate and fast MAS together with GIPAW (CASTEP) calculations enable the assignment of the ^{1}H, ^{13}C and ^{14}N/^{15}N resonances. A two-dimensional ^{1}H-^{1}H double-quantum (DQ) –single-quantum (SQ) MAS spectrum recorded with BaBa recoupling at 60 kHz MAS identifies specific proton-proton proximities associated with citrate-citrate and citrate-diethylcarbamazine intermolecular interactions.

Keywords: ^{1}H NMR, diethylcarbamazine citrate, salt, GIPAW calculations, fast MAS NMR

Graphical Abstract

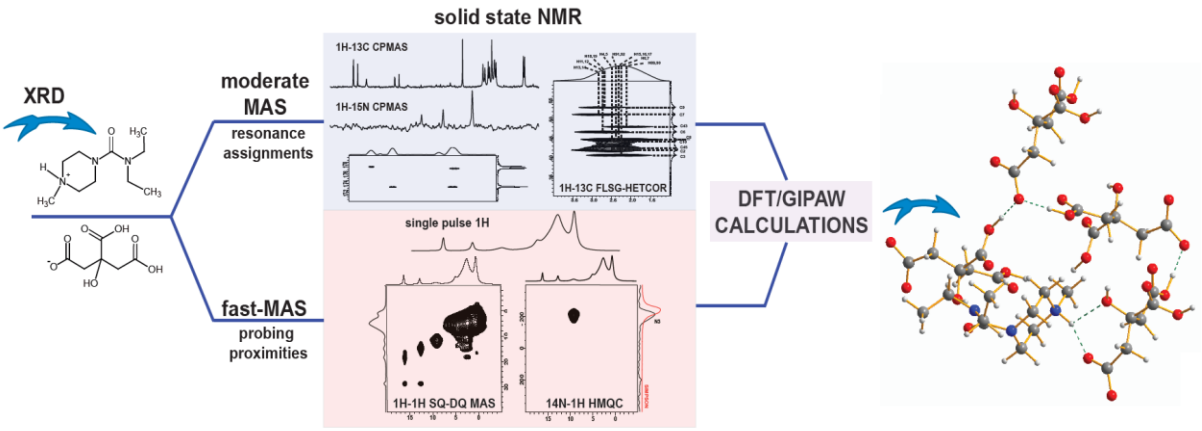

Highlights

- Fast MAS NMR and GIPAW calculations provide chemical shift assignments
- 1D ^{1}H fast MAS gives well resolved resonances for hydrogen bonded protons
- Intermolecular interactions revealed by fast MAS 2D ^{1}H-^{1}H DQ-SQ spectroscopy
- Strong citrate-citrate and weak diethylcarbamazine-citrate interactions are observed

* Corresponding author:
Fax: +55 16 3351-8350
E-mail address: venancio@ufscar.br (T. Venâncio).

Introduction

Diethylcarbamazine (1-(N,N-diethylcarbamoyl)-4-methylpiperazine, DEC) is currently the first option drug for treating filariasis, a serious disease caused by *Wuchereria bancrofti*, a nematode worm transmitted by different types of mosquitoes, common in tropical countries [1]. Among many other symptoms, the main characteristic of this disease, if not-treated, is a massive and chronic swelling in the limbs, due to the presence of adult worms in the lymphatic vessels that cause serious inflammation – at this stage the disease is called elephantiasis. The use of the free form of DEC in tablet formulations is not possible because of its very low thermal stability, with the melting point being around 40-45 $^{\circ}$C [2, 3]. To circumvent this limitation, a salt can be prepared by reacting citric acid with the DEC free base, resulting in the formation of a diethylcarbamazine dihydrogen citrate salt, i.e., a $(DEC)^{+}(citrate)^{-}$ salt [4]. This compound is stable up to significantly higher temperatures and it is quite common for a table salt enriched with DEC-citrate to be prescribed, in order to improve the adherence of the patients to the treatment [3, 5, 6].

Although this compound has been used since 60 years ago (at least), the crystal structure was only recently determined by Silva et al. in 2010 [4], by using single-crystal and powder X-Ray diffraction (PXRD). The $(DEC)^{+}(citrate)^{-}$ salt crystallizes in the centrosymmetric monoclinic $P2_1/c$ space group and the asymmetric unit contains one ionic pair of $(DEC)^{+}$ and $(citrate)^{-}$. The characterization of this type of compound is interesting for pharmaceutical companies, since such use offers a strategy to improve the solubility and/or the thermal stability of an active pharmaceutical ingredient [7, 8]. In this context, the $(DEC)^{+}(citrate)^{-}$ salt, as an example of a complex molecular packing, is a good target for the application of a combined experimental NMR and calculation approach [9-14]. Notably, this approach benefits greatly from the development since the late 1990s of NMR experiments under fast magic angle spinning (MAS). [15-18]

In this paper, ^{1}H MAS NMR techniques are used to investigate the solid-state structure of the $(DEC)^{+}(citrate)^{-}$ salt. Specifically, a ^{1}H-^{1}H double-quantum (DQ)- single-quantum (SQ) MAS NMR experiment [19-25] using BaBa recoupling experiment probes hydrogen-hydrogen proximities, mediated by homonuclear dipolar couplings. Additionally, fast MAS was employed to record a ^{14}N-^{1}H HMQC NMR spectrum that probes the ^{14}N quadrupolar interaction of the protonated nitrogen [26-28]. A 2D ^{1}H-^{13}C heteronuclear correlation

(HETCOR) MAS NMR spectrum recorded using cross polarisation (CP) transfer and Frequency Switched Lee-Goldburg (FSLG) ^{1}H-^{1}H homonuclear decoupling, ^{1}H-^{13}C CP-FSLG-HETCOR [29], was especially useful for assigning the DEC methylene protons and for probing proximities to non-protonated carbons in $(DEC)^{+}$ and $(citrate)^{-}$ ions. The solid-state NMR experiments are complemented by the calculation of NMR parameters using the GIPAW method.

Experimental and computational methods

NMR Experiments

Sample and packing: the active pharmaceutical ingredient, diethylcarbamazine citrate, was kindly donated by Fundação Oswaldo Cruz – Farmanguinhos, Rio de Janeiro, and used as received. Phase purity was verified by powder X-Ray diffraction and the data was recorded at room temperature using a Rigaku D/MAX 200 diffractometer (with a rotatory anode operating at 150 kV and 40 mA) operating with monochromatic Cu Kα radiation (Kα λ = 1.5406 Å). Approximately 1 and 60 mg of the powdered sample were packed into a 1.3 and 4 mm zirconia MAS NMR rotor, respectively.

Proton detected MAS NMR experiments: experiments were performed using a triple resonance probehead (HXY) for 1.3 mm rotors at a spinning frequency of 60 kHz. The bearing and drive gases were at room temperature – taking into account sample heating due to MAS [30], we estimate the sample temperature to correspond to ~50 °C.

The data were collected using a Bruker Avance II+ spectrometer operating with a 14.1 T wide bore magnet (600 MHz for ^{1}H resonance frequency). The ^{1}H 90º pulse duration was 2.5 μs corresponding to a nutation frequency of 100 kHz. Natural abundance *L*-alanine was employed for ^{1}H chemical shift referencing with respect to tetramethylsilane using the methyl group resonance at 1.1 ppm that corresponds to 1.85 ppm for adamantane [31].

2D ^{1}H double quantum (DQ) MAS NMR experiment: One rotor period of the back to back (BaBa) [32, 33] recoupling sequence was used for the excitation and reconversion of DQ coherences. A 16-step phase cycle was used in order to select $\Delta p = \pm 2$ on the DQ excitation pulses (4 steps) and $\Delta p = -1$ (4 steps) on the *z*-filter 90° pulse, where *p* is the coherence

order. 16 transients were coadded for each of 160 t_1 FIDs, using the States method to achieve sign discrimination in F_1 with a rotor-synchronized t_1 increment of 16.7 μs. The total experimental time was 4.3 h using a recycle delay of 6 s.

2D ^{14}N-^{1}H heteronuclear multiple quantum correlation (HMQC) MAS NMR experiment: a modified version of the ^{14}N–^{1}H HMQC pulse sequence of Gan et al [34] employing rotary resonance recoupling (R^3) [35] was used. The modification consists of applying a second ^{1}H 90° pulse (90° out of phase with respect to the first 90° pulse) immediately after the first ^{1}H 90° pulse and using phase inversion (every rotor period) of the $n = 2$ ($\nu_1 = 2\ \nu_R$) rotary-resonance recoupling pulses [36] . A four-step nested phase cycle was used to select changes in coherence order $\Delta p = \pm 1$ (on the first ^{1}H pulse, 2 steps) and $\Delta p = -1$ (on the last ^{14}N pulse, 2 steps). The recoupling duration was 4 τ_R = 66.8 μs. The ^{14}N pulse duration was 5 μs. For each of 64 t_1 FIDs (using the States method to achieve sign discrimination in F_1 with a rotor synchronized increment of 16.7 μs), 64 transients were co-added with a recycle delay of 6 s, corresponding to a total experimental time of 7 h.

^{13}C and ^{15}N detected CP MAS NMR experiments: ^{1}H-^{13}C and ^{1}H-^{15}N CPMAS experiments were performed using a Bruker Avance III spectrometer operating with a narrow bore 11.7 T magnet (500 MHz for ^{1}H resonance frequency) and equipped with a HX probehead for 4 mm rotors. A MAS frequency of 5 kHz was used. A two-pulse phase-modulated TPPM-15 scheme [37, 38] was used for ^{1}H decoupling at a nutation frequency of 100 kHz. Cross polarization was applied by using a 90-100% amplitude ramp on ^{1}H [39] during a contact time of 2 ms (for ^{13}C) or 4 ms (for ^{15}N). 256 (for ^{13}C) or 4096 (for ^{15}N) transients were coadded with a recycle delay of 3 s. For ^{13}C, adamantane was used as an external reference for tetramethylsilane (TMS), setting the CH_2 signal to 38.5 ppm [31, 40]. For ^{15}N, glycine was used as an external reference (–347.4 ppm, related to nitromethane) [41]. To convert to the chemical shift scale frequently used in protein NMR, where the alternative IUPAC reference [42] is liquid ammonia at –50 °C, it is necessary to add 379.5 to the given values [43].

2D CP - ^{1}H (FSLG)-^{13}C Heteronuclear Correlation MAS NMR [29]: the experiment was performed using a Bruker Avance III spectrometer operating with a wide bore 11.7 T magnet (500 MHz for ^{1}H resonance frequency) and using a 4 mm HXY probehead at a MAS

frequency of 12.5 kHz. Both homonuclear (FSLG, [44, 45]) and heteronuclear SPINAL-64 [46] ^{1}H decoupling employed a nutation frequency of 100 kHz. For each of 128 t_1 FIDs (using the States method to achieve sign discrimination in F_1 with a rotor synchronized increment of 80 μs), 16 transients were coadded with a recycle delay of 11 s corresponding to a total experimental time of 6.5 h. For CP (contact time of 200 μs), a 90-100% amplitude ramp on ^{1}H was employed. ^{13}C chemical shifts were referenced using *L*-alanine as an external reference (using the CH_3 signal centred at 20.5 ppm), corresponding to the same adamantane reference referred to above. The FSLG scaling factor in the ^{1}H chemical shift axis was 0.56 with the ^{1}H chemical shifts being referenced according to the fast MAS spectrum.

DFT GIPAW Calculations:

Calculations were performed by employing a plane-wave based DFT approach as implemented in the CASTEP code, UK academic release version 8.0 [47]. Initial atomic coordinates were taken from the published crystal structure [4] for which the ".cif" file is available on the Crystallography Open Database http://www.crystallography.net/cod/cod/4501669.html, with code 4501669: Space Group $P2_1/c$, $Z = 4$, $Z' = 0$, 224 atoms in the unit cell, cell dimensions (Å): $a = 13.8050$, $b = 10.2581$; $c = 13.9890$, cell angles (°): $\alpha = 90.00$, $\beta = 93.689$ and $\gamma = 90.00$; cell volume $V = 1976.92$ Å^3. A new ".cif" file was created from the original one to describe only the conformer with the higher probability (70%, conformer 1), i.e., the C7A', C8A', H8A1', H8A2', H8A3', H7A1' and H7A2' atoms were manually deleted.

The unit cell parameters were fixed, space group symmetry was imposed, and periodic boundary conditions were applied during the geometry optimization. NMR shielding calculations were performed using the gauge-including projector-augmented wave (GIPAW) approach [48, 49]. Both geometry optimizations and NMR chemical shift calculations used a plane-wave basis set and the PBE exchange correlation functional [49, 50] at a basis cut-off energy of 700 eV with integrals taken over the Brillouin zone by using a Monkhorst−Pack grid of minimum sample spacing $0.1 \times 2\pi$ Å^{-1}. A semi empirical dispersion correction was applied using the TS scheme [51] during both geometry optimization and NMR shielding calculations, employing ultrasoft pseudopotentials generated on the fly (OTF) [52]. After geometry optimization, the forces, energies and displacements were better than 0.05 eV Å^{-1},

0.000002 eV and 0.0002 Å, respectively. Distances stated in this paper are for the geometry-optimised structure. GIPAW calculated NMR shielding were visualized, processed, and tabulated through the CCP-NC output files visualization tool, MagresView version 1.6 [53], running on Mozilla Firefox web browser version 49.0.2.

Results and discussion

Chemical shift assignments

One-dimensional ^{1}H (one-pulse), ^{13}C and ^{15}N (CP MAS) spectra of diethylcarbamazine citrate are presented in Figure 1, while Table 1 compares experimental and calculated (GIPAW) ^{1}H, ^{13}C and ^{15}N chemical shifts. Note that the geometry optimisation within CASTEP causes a relabelling of the atoms – in this paper, we use the CASTEP numbering; see Table 1 below for a comparison with the numbering employed in the crystallographic cif file. It is a well known phenomenon [10, 14] that the gradient of a plot of experimental ^{13}C chemical shift against calculated shielding deviates slightly from minus one [54]. Thus, in this work, to enable a clearer comparison between experimental and GIPAW calculated ^{13}C chemical shifts, we use an approach previously employed in Ref. [55], whereby there are two different reference shieldings for calculated ^{13}C isotropic chemical shifts above and below 70 ppm.

The assignment of the experimental ^{1}H chemical shifts is based on a 2D ^{1}H-^{13}C correlation spectrum in Figure 2b (expanded in Figure 3) that was recorded with a CP-HETCOR experiment employing FSLG ^{1}H decoupling. The use of CP to establish a heteronuclear correlation based on through-space ^{1}H-^{13}C dipolar couplings is beneficial for the observation of cross peaks for CH_2 moieties that usually have low sensitivity in a *J*-based ^{1}H-^{13}C refocused INEPT spectrum[55, 56]. Such a refocused INEPT ^{1}H-^{13}C correlation spectrum is (for a short spin-echo duration) usually selective for one-bond C-H connectivities. By contrast, we observe that the use here of CP, even for a relatively short contact time of 200 μs, results in the observation of albeit low-intensity cross peaks corresponding to longer-range C-H proximities in Figure 2b and 3. In this way, cross peaks for the intramolecular longer-range C-H proximities involving the carboxylic acid (C41 and C46), carboxylate (C44) and quaternary (C42) citric acid carbons are revealed. Specifically, as shown in Figure 3, cross peaks are observed for the COOH groups, C41 with H93 (1.98 Å)

and C46 with H95 (1.93 Å). For the carboxylate C44, cross peaks are observed with the C43 CH_2 protons (distances of 2.13 (H89) and 2.15 (H90) Å), while for the central quaternary carbon C42, cross peaks are observed to the OH proton (H94, 1.98 Å) and the C43 and C45 CH_2 groups (H89 to H92, distances between 2.14 and 2.18 Å).

As well as the ^{15}N CP MAS spectrum presented in Figure 1, a ^{14}N-^{1}H HMQC spectrum is presented in Figure 2c. This two-dimensional ^{14}N-^{1}H spectrum was recorded with a short duration of rotary resonance recoupling such that a cross peak is only observed for the protonated N3 nitrogen. For the spin $I = 1$ nucleus, ^{14}N, there is line broadening due to the second-order quadrupolar interaction and the ^{14}N shift depends on the sum of the isotropic chemical shift and the isotropic second-order quadrupolar shift. The red spectrum to the right of Figure 3c corresponds to a simulation using the calculated (GIPAW) quadrupolar parameters (see Table S1); good agreement to experiment is evident.

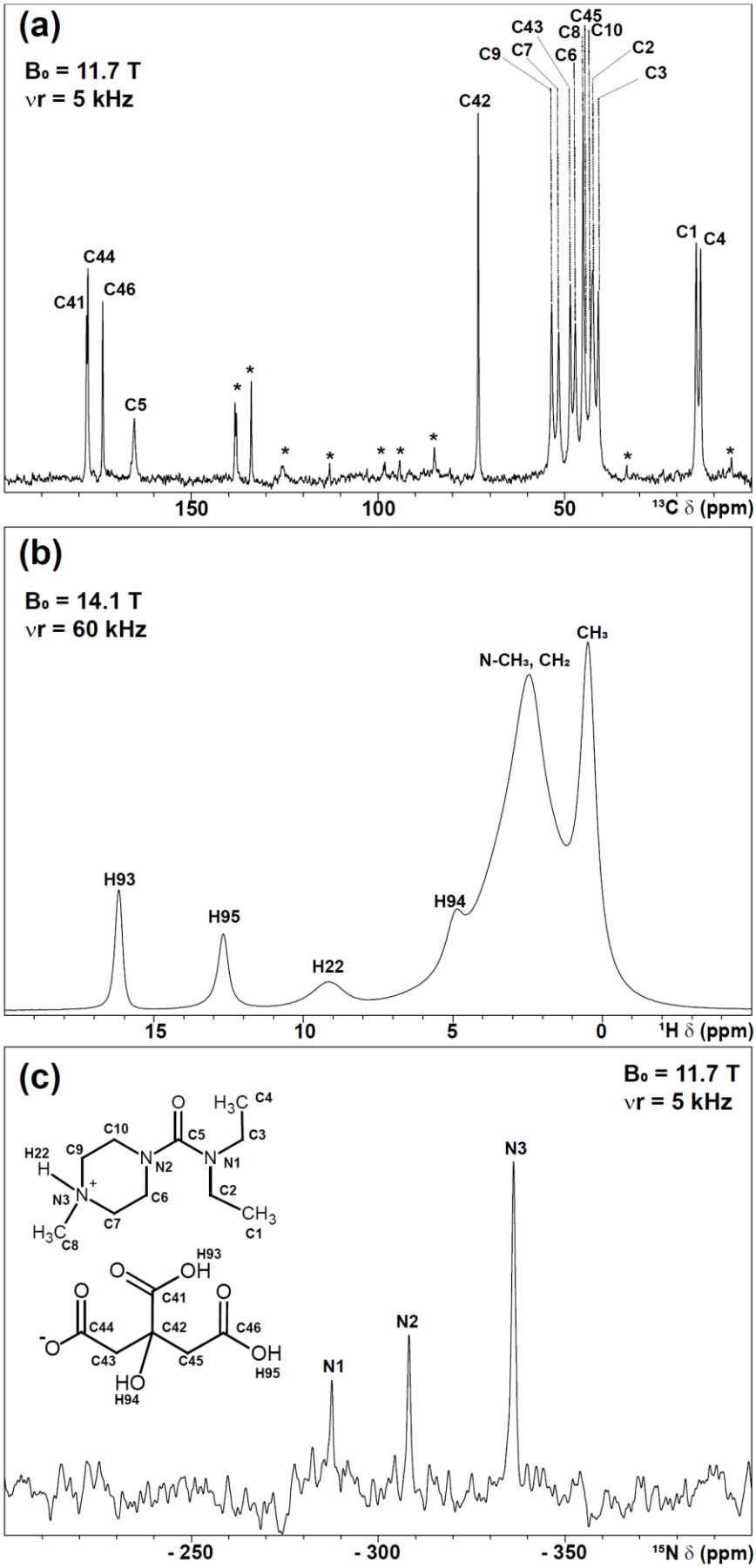
(a)
B₀ = 11.7 T
νr = 5 kHz
C45
C43
C8
C10
C9
C7
C6
C2
C3
C42
C1
C4
C44
C41
C46
C5
150
100
50
¹³C δ (ppm)
(b)
B₀ = 14.1 T
νr = 60 kHz
CH₃
N-CH₃, CH₂
H93
H95
H22
H94
15
10
5
0
¹H δ (ppm)
(c)
B₀ = 11.7 T
νr = 5 kHz
N3
N2
N1
- 250
- 300
- 350
¹⁵N δ (ppm)

1

Figure 1: One-dimensional solid-state MAS NMR spectra of the diethylcarbamazine citrate salt: (a) a ^{1}H (500 MHz)-^{13}C CP MAS (5 kHz) spectrum; (b) a ^{1}H (600 MHz) single-pulse MAS (60 kHz) spectrum (8 co-transients were added for a recycle delay of 6 s); (c) a ^{1}H (500 MHz)-^{15}N CP MAS (5 kHz) spectrum. Asterisks denote spinning sidebands in (a).

Table 1: Experimental and calculated (GIPAW) isotropic chemical shifts (in ppm) for the diethycarbamazine citrate salt.

LABELLING		**Atom descriptor**	**GIPAW calculation[a]**	**Experimental**
CASTEP	**X-Ray [4]**		**δ_{iso}**	**δ_{iso}**
C1	C10A	CH_3	10.9	14.2
C2	C9A	CH_2	42.0	42.1
C3	C7A	CH_2	40.5	40.7
C4	C8A	CH_3	8.6	13.6
C5	C6A	C=O	163.0	164.9
C6	C4A	CH_2	49.3	48.2
C7	C3A	CH_2	50.9	51.3
C8	C5A	CH_3	44.2	44.8
C9	C2A	CH_2	53.0	53.2
C10	C1A	CH_2	43.4	44.5
C41	C6C	COOH	180.9	177.6
C42	C3C	C_{quat}	74.2	72.8
C43	C2C	CH_2	49.1	46.8
C44	C1C	COO^-	179.3	177.3
C45	C4C	CH_2	42.6	42.4
C46	C5C	COOH	176.3	173.3
H1,H2,H3	H10A1,H10A2,H10A3	CH_3	0.4	0.5
H4	H9A1	CH_2	2.5	2.5
H5	H9A2	CH_2	2.3	
H6	H7A1	CH_2	2.1	2.3
H7	H7A2	CH_2	2.5	
H8, H9, H10	H8A1, H8A2, H8A3	CH_3	0.1[b]	0.5
H11	H4A1	CH_2	2.7	2.7
H12	H4A2	CH_2	2.8	
H13	H3A1	CH_2	2.9	2.8
H14	H3A2	CH_2	3.3	
H15, H16, H17	H5A1, H5A2, H5A3	CH_3	2.1[b]	2.3
H18	H2A1	CH_2	2.4	2.7
H19	H2A2	CH_2	3.0	

H20	H1A1	CH_2	3.6	2.9
H21	H1A2	CH_2	2.7	
H22	H2A	N^+H	9.4	9.1
H89	H2C1	CH_2	1.6	2.1
H90	H2C1	CH_2	2.3	
H91	H4C1	CH_2	2.5	2.7
H92	H4C2	CH_2	2.1	
H93	H6C	COOH	16.7	16.2
H94	H3C	OH	4.2	4.8
H95	H7C	COOH	14.3	12.8
N1	N2A	N(C=O)N	–286.8	–287.7
N2	N1A	N(C=O)N	–309.4	–308.4
N3	N3A	N^+H	–328.6	–336.4

[a] Calculated isotropic chemical shifts are given by $\delta_{iso}^{calc} = \sigma_{ref} - \sigma_{calc}$, where σ_{ref} is 30 ppm for ^1H and –153 ppm for $^{14}N/^{15}N$. For ^{13}C two shielding references were used: σ_{ref} = 170 ppm for $\delta_{iso} > 70$ ppm and σ_{ref} = 173 ppm for $\delta_{iso} < 70$ ppm [55].

[b] For CH_3 groups, the stated calculated isotropic ^1H chemical shift corresponds to the average for the three protons.

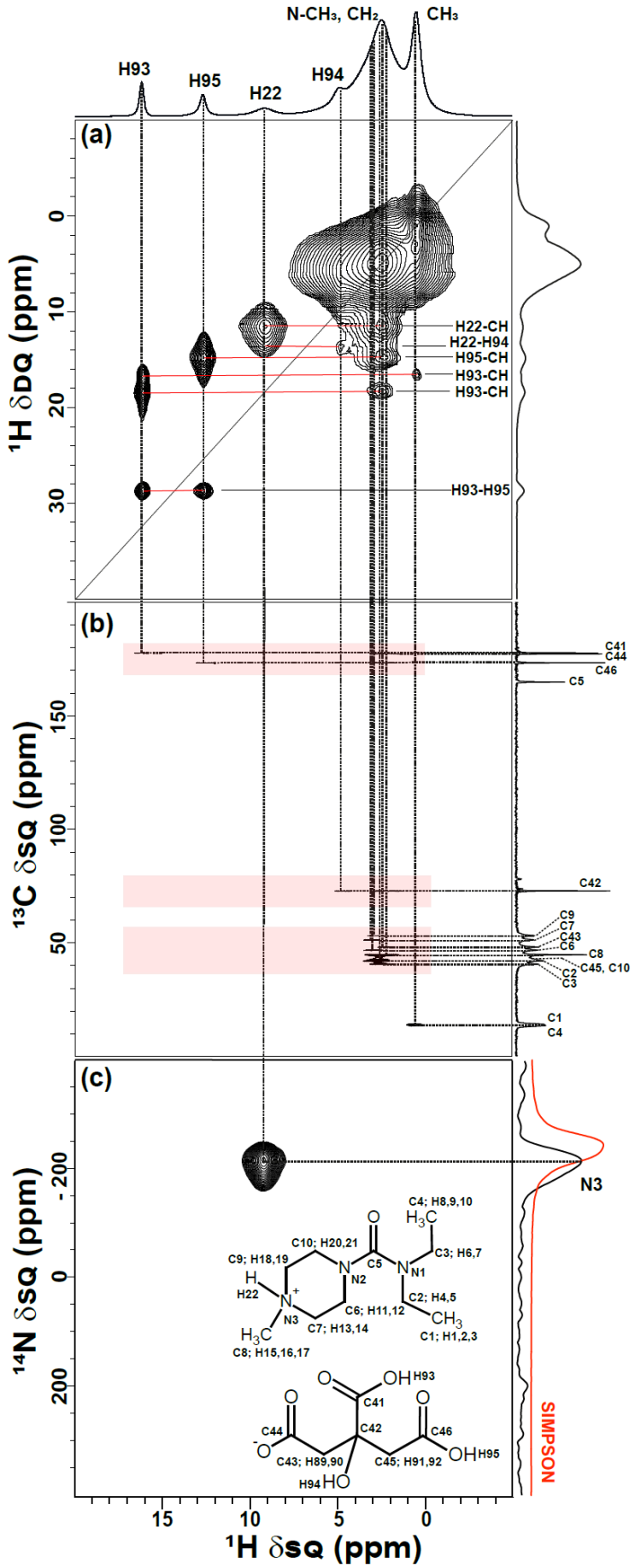
N-CH₃, CH₂
CH₃
H93
H95
H22
H94
(a)
¹H δDQ (ppm)
H22-CH
H22-H94
H95-CH
H93-CH
H93-CH
H93-H95
(b)
¹³C δSQ (ppm)
C41
C44
C46
C5
C42
C9
C7
C43
C6
C8
C2
C45, C10
C3
C1
C4
(c)
¹⁴N δSQ (ppm)
N3
C4; H8,9,10
C10; H20,21
C3; H6,7
C9; H18,19
C5
N1
N2
C2; H4,5
H22
N3
C6; H11,12
C7; H13,14
C1; H1,2,3
C8; H15,16,17
OH H93
C41
C44
C42
C46
C43; H89,90
C45; H91,92
OH H95
H94 HO
SIMPSON
¹H δSQ (ppm)

1

Figure 2: 2D solid-state MAS NMR spectra of the diethylcarbamazine citrate salt: (a) a ^{1}H-^{1}H (600 MHz) DQ-SQ MAS (60 kHz) correlation spectrum with skyline projections recorded using one rotor period of BaBa recoupling; (b) a ^{1}H (500 MHz)-^{13}C HETCOR MAS (12.5 kHz) spectrum (together with a F_1 skyline projection) recorded using FSLG ^{1}H decoupling and a CP contact time of 200 μs (red shaded rectangles indicate the regions for which zoomed-in views are presented in Figure 3); (c) a ^{14}N-^{1}H (600 MHz) HMQC MAS (60 kHz) spectrum recorded using four rotor periods of rotary resonance recoupling – on the right-hand side, the skyline projection is compared to a spectrum simulated using the GIPAW calculated NMR parameters (see a SIMPSON [57] input file (in the Supporting Information) for N3). The base contour is at (a) 10%, (b) 20% and (c) 20% of the maximum intensity.

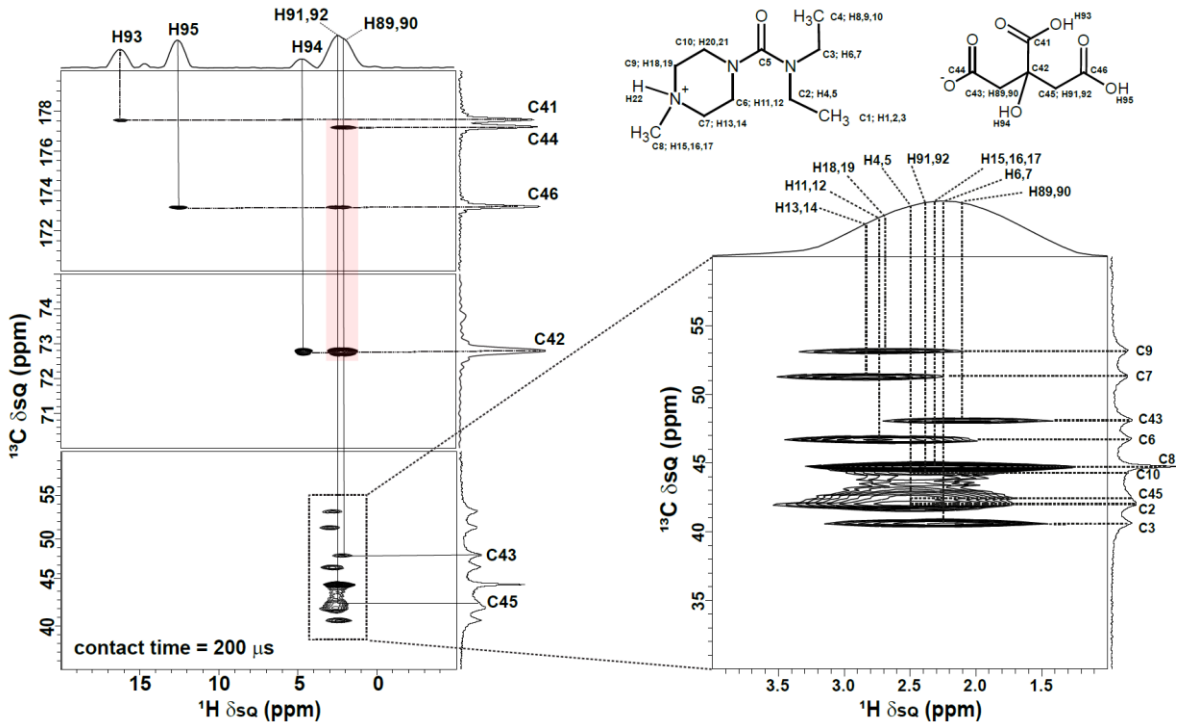

Figure 3: Zoomed-in regions for the ^{1}H-^{13}C HETCOR spectrum of the diethylcarbamazine citrate salt presented in Figure 2b, together with skyline projections.

Proton-proton proximities

^{1}H solid-state NMR experiments performed under fast MAS are a powerful probe of intermolecular hydrogen bonding arrangements, with the ^{1}H chemical shift being a sensitive indicator of hydrogen-bonding strength. In particular, two-dimensional ^{1}H DQ MAS spectra provide valuable insight into proton-proton proximities of such hydrogen-bonded protons. A 2D ^{1}H-^{1}H DQ-SQ spectrum of the diethylcarbamazine citrate salt recorded at fast MAS is presented in Figure 2a. There are two ^{1}H resonances with chemical shifts above 10 ppm in Figure 1b, at 16.2 and 12.8 ppm. On the basis of the ^{1}H-^{13}C HETCOR spectrum (see Figure 2b and 3) and the GIPAW chemical shielding calculations, these are assigned to the H93 (16.2 ppm) and H95 (12.8 ppm) protons of the C41 and C46 COOH groups. As shown in Figure 4 (views a and b), both COOH protons form an intermolecular OH…O hydrogen bonding to the same oxygen atom (O8) of the C44 carboxylate group, i.e., the O8 oxygen atom exhibits bifurcated hydrogen bonding. Both OH…O hydrogen bonds are close to linear (175.6° and 177.0°): for H93 which has the ^{1}H higher chemical shift, the hydrogen bond has slightly shorter H…O (1.48 Å compared to 1.56 Å) and O…O (2.54 Å compared to 2.59 Å) distances than that of H95. Note that the difference in experimental ^{1}H chemical shifts of 3.4 ppm (16.2 as compared to 12.8 ppm) is slightly bigger than that for the calculated (GIPAW) ^{1}H chemical shifts (2.4 ppm, 16.7 as compared to 14.3 ppm, see Table 1). In this respect, it is known that experimental ^{1}H chemical shifts of hydrogen-bonded protons increase upon decreasing temperature [58] further noting that GIPAW calculations correspond to 0 K. Note that there is no evident hydrogen bonding for the two other oxygen atoms (O6 or O10) attached to the same carbon atoms (C41 and C46) as the H93 or H95 OH groups that could explain the large difference in the ^{1}H higher chemical shifts of H93 or H95.

The bifurcated hydrogen bonding of the carboxylate O8 oxygen with the two COOH groups leads to a close proximity of the H93 and H95 COOH protons (2.50 Å, see Table 2), with a cross peak being observed at a ^{1}H DQ frequency of 16.2 + 12.8 = 29.0 ppm in Figure 2a. DQ peaks are also observed for H93 and H95 with aliphatic protons (see Figure 2a and Table 2), notably, H95 has a close intermolecular proximity (2.29 Å) to the citrate CH_2 H90 proton (see Figure 4a).

Consider the diethylcarbamazine NH^+ H22 proton. As shown in Figure 4c, this has a close proximity to two hydrogen bond donor atoms, namely the other oxygen (O9) of the citrate carboxylate group and the oxygen (O5) of the citric acid OH group. While the N3…O5

distance (2.92 Å) is only slightly longer than the N3…O9 distance (2.76 Å), the NHO angle is an unfavourable 116.7° for the OH O5 as compared to 150.7° for the carboxylate O9, resulting in a significantly longer H..O distance of 2.28 Å as compared to 1.79 Å. The experimental ^{1}H chemical shift for the diethylcarbamazine NH^{+} H22 proton of 9.1 ppm is in good agreement with the calculated (GIPAW) value of 9.4 ppm. Looking at the ^{1}H DQ MAS spectrum in Figure 2a, it is interesting to observe a resolved weak cross peak at the OH single-quantum frequency between the H22 and the OH H94 proton at a ^{1}H DQ frequency of 9.1 + 4.8 = 13.9 ppm, corresponding to a H-H distance of 3.05 Å. The low ^{1}H chemical shift for the citric acid OH moiety of 4.8 ppm is consistent with it forming a hydrogen bond to the DEC carbonyl oxygen with a relatively long O…O and H…O distance of 2.81 and 1.95 Å, respectively (OHO bond angle of 144.3°).

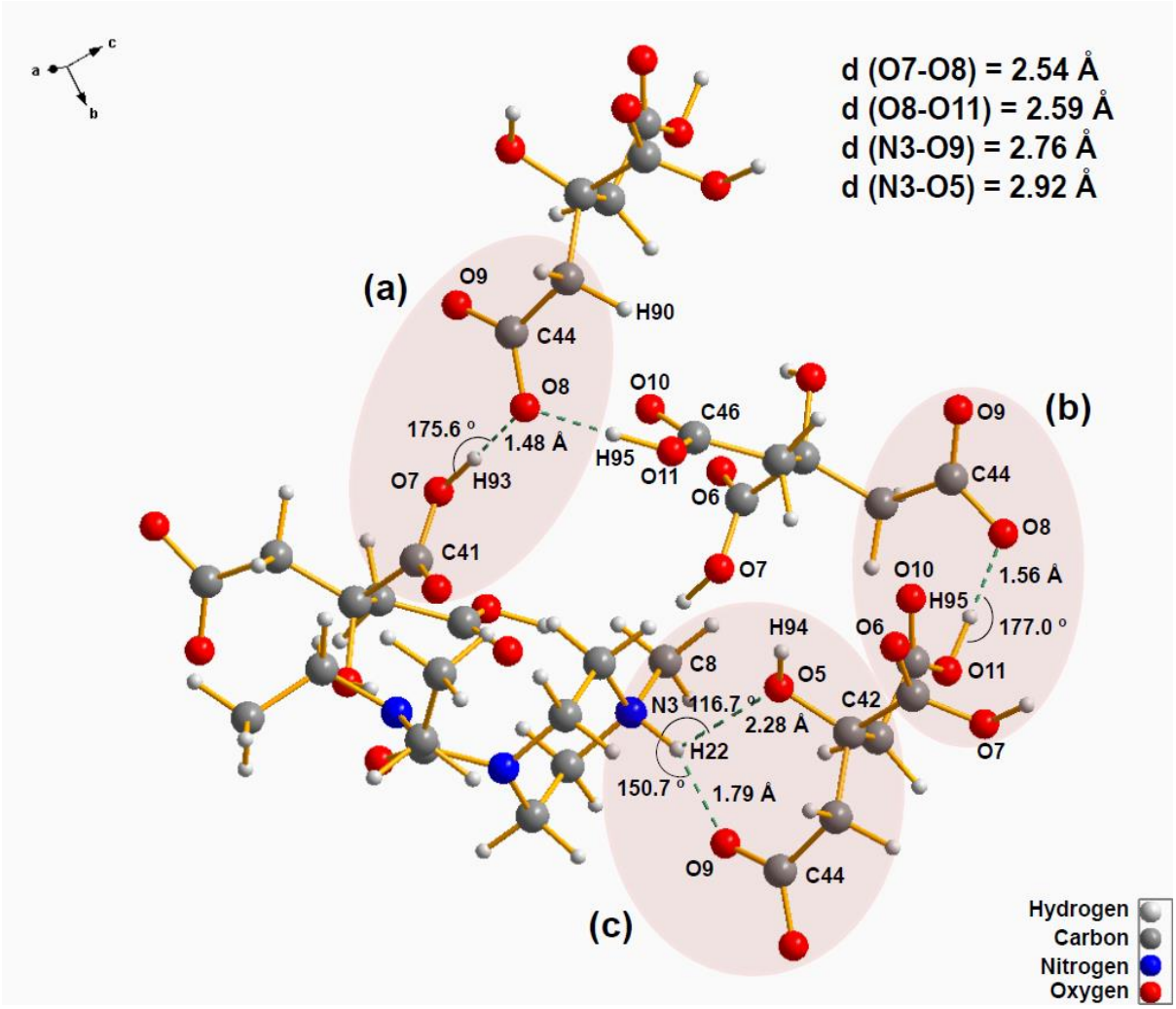

Figure 4: A representation of the geometry-optimised (CASTEP) crystal structure of the diethylcarbamazine citrate salt, focusing on the intermolecular hydrogen-bonding interactions. X…Y and H…Y distances and XHY angles are stated for the XH…Y

intermolecular hydrogen bonding exhibited by the (a, b) citrate COOH and (c) diethylcarbamazine NH^+ groups.

Table 2. H-H proximities (< 3.5 Å) and corresponding ^{1}H DQ shifts (see Fig. 2a) for the NH, OH, COOH and CH protons in the diethylcarbamazine citrate salt.

atom	**H-H proximity**	**δ_{iso}^{exp} SQ / ppm**	**δ^{exp} DQ / ppm**	**H-H distance[a] (Å)**
H93, C(41)OOH	*H95 (C(46)OOH)*	*12.8*	*29.0*	*2.50*
16.2 ppm	*H3 (C1, CH_3)*	*0.5*	*16.7*	*2.78*
	H2 (C1, CH_3)	*0.5*	*16.7*	*3.01*
	H16 (C8, CH_3)	*2.3*	*18.5*	*3.03*
	H15 (C8, CH_3)	*2.3*	*18.5*	*3.14*
	H90 (C43, CH_2)	2.5	18.7	3.37
H95, C(46)OOH	*H90 (C43, CH_2)*	*2.5*	*15.3*	*2.29*
12.8 ppm	*H93 (C(41)OOH)*	*16.2*	*29.0*	*2.50*
	H20 (C10, CH_2)	*2.9*	*15.7*	*3.03*
	H10 (C4, CH_3)	*0.5*	*(13.3)*	*3.34*
	H15 (C8, CH_3)	*2.3*	*15.1*	*3.45*
	H89 (C43, CH_2)	*2.5*	*15.3*	*3.46*
	H13 (C7, CH_2)	*2.8*	*15.6*	*3.49*
H22, N(3)$^+$H	H18 (C9, CH_2)	2.7	11.8	2.34
9.1 ppm	H17 (C8, CH_3)	2.3	11.4	2.38
	H16 (C8, CH_3)	2.3	11.5	2.39
	H14 (C7, CH_2)	2.8	11.9	2.40
	H21 (C10, CH2)	2.9	12.0	2.53
	H11 (C6, CH_2)	2.7	11.8	2.56
	H91 (C45, CH_2)	*2.7*	*11.8*	*2.72*
	H19 (C9, CH_2)	2.7	11.8	2.96
	H15 (C8, CH_3)	2.3	11.4	2.97
	H13 (C7, CH_2)	2.8	11.9	2.98

	H94 (OH)	*4.8*	*13.9*	*3.05*
H94, O(5)H	*H14 (C7, CH_2)*	*2.8*	*7.6*	*2.39*
4.8 ppm	*H19 (C9, CH_2)*	*2.7*	*7.5*	*2.67*
	H7 (C3, CH_2)	*2.3*	*7.1*	*2.80*
	H89 (C43, CH_2)	2.5	*7.3*	2.82
	H22 (N^+H)	*9.1*	*13.6*	*3.05*
	H17 (C8, CH_3)	*2.3*	*7.1*	*3.12*
	H11 (C6, CH_2)	*2.7*	*7.5*	*3.34*
	H91 (C45, CH_2)	2.7	*7.5*	3.46
	H20 (C10, CH_2)	*2.9*	*7.7*	*3.47*

[a] H-H distances are taken from the DFT (CASTEP) optimized structure. Intermolecular proximities are denoted using italic font.

Conclusions

Fast MAS ^{1}H NMR experiments have been used in conjunction with GIPAW calculation to probe intermolecular interactions in a diethylcarbamazine citrate salt. Notably, 1D and 2D ^{1}H solid state experiments recorded under fast MAS (60 kHz) or at moderate MAS with ^{1}H homonuclear decoupling (FSLG) combined with the GIPAW calculation of NMR parameters enabled an assignment of the ^{1}H, ^{13}C and ^{15}N chemical shifts. These findings reinforce the use of NMR crystallography to characterize pharmaceutical supramolecular complexes, with special attention to co-crystals and salts, whose use has been growing more recently. The design of new drugs and formulations as well as the co-formulation of two (or more) drugs offers many challenges in terms of packing complexity and molecular dynamics.

Acknowledgements

We would like to acknowledge Fundação Osvaldo Cruz – Instituto de Tecnologia de Fármacos -Farmanguinhos for providing the sample used in this work. CASTEP calculations were performed at the University of Warwick Scientific Computing Research Technology Platform. T. V. thanks the Fundação de Amparo à Pesquisa do Estado de São Paulo (FAPESP, processes: 2009/13860-2 and 2015/21708-7) and INCP-CBIP/UFSCar, while

L.M.A.M. thanks CNPq (process: 142384/2010-0). Prof. Dr. Emerson Rodrigues de Carmargo is thanked for collecting X-Ray data. The calculated and experimental data for this study are provided as a supporting dataset from WRAP, the Warwick Research Archive Portal at http://wrap.warwick.ac.uk/***.

Supporting Information

Experimental and calculated PXRD for the diethylcarbamazine citrate salt; GIPAW DFT calculated electric field gradient tensors, quadrupolar interaction parameters and calculated and experimental isotropic shifts for ^{14}N; input parameters for ^{14}N lineshape SIMPSON simulations as well as SIMPSON simulated ^{14}N lineshapes for the diethylcarbamazine citrate salt (pdf). The ".cif" and ".magres" files are also available.

References

[1] E. Kimura, J.U. Mataika, Control of lymphatic filariasis by annual single-dose diethylcarbamazine treatments, Parasitol Today, 12 (1996) 240-244.
[2] L.L. Chaves, L.A. Rolim, M. Goncalves, A.C.C. Vieira, L.D.S. Alves, M.F.R. Soares, J.L. Soares-Sobrinho, M.C.A. Lima, P.J. Rolim-Neto, Study of stability and drug-excipient compatibility of diethylcarbamazine citrate, J. Therm. Anal. Calorim., 111 (2013) 2179-2186.
[3] S.B. Honorato, C.C.P. da Silva, Y.S. de Oliveira, J.S. Mendonca, N. Boechat, J. Ellena, A.P. Ayala, On the thermal stability of the diethylcarbamazine-fortified table salt used in the control of lymphatic filariasis, J. Pharm. Sci., 105 (2016) 2437-2443.
[4] C.C.P. da Silva, F.T. Martins, S.B. Honorato, N. Boechat, A.P. Ayala, J. Ellena, Triple structural transition below room temperature in the antifilarial drug diethylcarbamazine citrate, Cryst. Growth Des., 10 (2010) 3094-3101.
[5] A. Davis, D.R. Bailey, Effect of salt medicated with diethylcarbamazine in bancroftian filariasis, Bull. World Health Organ., 41 (1969) 195-208.
[6] A. Weaver, P. Brown, S. Huey, M. Magallon, E.B. Bollman, D. Mares, T.G. Streit, M. Lieberman, A low-tech analytical method for diethylcarbamazine citrate in medicated salt, PLoS Negl.Trop. Dis., 5 (2011) e1005.
[7] K. Izutsu, T. Koide, N. Takata, Y. Ikeda, M. Ono, M. Inoue, T. Fukami, E. Yonemochi, Characterization and quality control of pharmaceutical cocrystals, Chem. Pharm. Bull., 64 (2016) 1421-1430.
[8] G. Bolla, A. Nangia, Pharmaceutical cocrystals: walking the talk, Chem. Commun., 52 (2016) 8342-8360.
[9] D.C. Apperley, A.S. Batsanov, S.J. Clark, R.K. Harris, P. Hodgkinson, D.B. Jochym, Computation of magnetic shielding to simultaneously validate a crystal structure and assign a solid-state NMR spectrum, J. Mol. Struct., 1015 (2012) 192-201.
[10] S.E. Ashbrook, D. McKay, Combining solid-state NMR spectroscopy with first-principles calculations - a guide to NMR crystallography, Chem. Commun., 52 (2016) 7186-7204.

[11] R.K. Harris, NMR crystallography: the use of chemical shifts, Solid State Sci., 6 (2004) 1025-1037.
[12] R.K. Harris, P. Hodgkinson, C.J. Pickard, J.R. Yates, V. Zorin, Chemical shift computations on a crystallographic basis: some reflections and comments, Magn. Reson. Chem., 45 (2007) S174-S186.
[13] B. Elena, G. Pintacuda, N. Mifsud, L. Emsley, Molecular structure determination in powders by NMR crystallography from proton spin diffusion, J. Am. Chem. Soc., 128 (2006) 9555-9560.
[14] C. Bonhomme, C. Gervais, F. Babonneau, C. Coelho, F. Pourpoint, T. Azais, S.E. Ashbrook, J.M. Griffin, J.R. Yates, F. Mauri, C.J. Pickard, First-principles calculation of NMR parameters using the Gauge Including Projector Augmented Wave method: A chemist's point of view, Chem. Rev., 112 (2012) 5733-5779.
[15] Y. Nishiyama, Fast magic-angle sample spinning solid-state NMR at 60-100 kHz for natural abundance samples, Solid State Nucl. Magn. Reson., 78 (2016) 24-36.
[16] Y. Nishiyama, Y. Endo, T. Nemoto, H. Utsumi, K. Yamauchi, K. Hioka, T. Asakura, Very fast magic angle spinning ^{1}H-^{14}N 2D solid-state NMR: Sub-micro-liter sample data collection in a few minutes, J. Magn. Reson., 208 (2011) 44-48.
[17] A. Samoson, T. Tuherm, Z. Gan, High-field high-speed MAS resolution enhancement in ^{1}H NMR spectroscopy of solids, Solid State Nucl. Magn. Reson., 20 (2001) 130-136.
[18] Y.Q. Ye, M. Malon, C. Martineau, F. Taulelle, Y. Nishiyama, Rapid measurement of multidimensional ^{1}H solid-state NMR spectra at ultra-fast MAS frequencies, J. Magn. Reson., 239 (2014) 75-80.
[19] M. Baias, A. Lesage, S. Aguado, J. Canivet, V. Moizan-Basle, N. Audebrand, D. Farrusseng, L. Emsley, Superstructure of a substituted zeolitic imidazolate metal-organic framework determined by combining proton solid-state NMR spectroscopy and DFT calculations, Angew. Chem. Int. Ed., 54 (2015) 5971-5976.
[20] J.A. Fernandes, M. Sardo, L. Mafra, D. Choquesillo-Lazarte, N. Masciocchi, X-Ray and NMR crystallography studies of novel theophylline cocrystals prepared by liquid assisted grinding, Cryst. Growth Des., 15 (2015) 3674-3683.
[21] M.R. Hansen, R. Graf, H.W. Spiess, Interplay of structure and dynamics in functional macromolecular and supramolecular systems as revealed by Magnetic Resonance Spectroscopy, Chem. Rev., 116 (2016) 1272-1308.
[22] J. Xu, V.V. Terskikh, Y.Y. Chu, A.M. Zheng, Y.N. Huang, Mapping out chemically similar, crystallographically nonequivalent hydrogen sites in metal-organic frameworks by ^{1}H solid-state NMR spectroscopy, Chem. Mater., 27 (2015) 3306-3316.
[23] S.P. Brown, Applications of high-resolution ^{1}H solid-state NMR, Solid State Nucl. Magn. Reson., 41 (2012) 1-27.
[24] L. Mafra, R. Siegel, C. Fernandez, D. Schneider, F. Aussenac, J. Rocha, High-resolution ^{1}H homonuclear dipolar recoupling NMR spectra of biological solids at MAS rates up to 67 kHz, J. Magn. Reson., 199 (2009) 111-114.
[25] L. Mafra, S.M. Santos, R. Siegel, I. Alves, F.A.A. Paz, D. Dudenko, H.W. Spiess, Packing interactions in hydrated and anhydrous forms of the antibiotic ciprofloxacin: a solid-state NMR, X-Ray Diffraction, and computer simulation study, J. Am. Chem. Soc., 134 (2012) 71-74.
[26] S. Cavadini, V. Vitzthum, S. Ulzega, A. Abraham, G. Bodenhausen, Line-narrowing in proton-detected nitrogen-14 NMR, J. Magn. Reson., 202 (2010) 57-63.
[27] A.S. Tatton, T.N. Pham, F.G. Vogt, D. Iuga, A.J. Edwards, S.P. Brown, Probing intermolecular interactions and nitrogen protonation in pharmaceuticals by novel ^{15}N-edited and 2D ^{14}N-^{1}H solid-state NMR, CrystEngComm, 14 (2012) 2654-2659.

[28] S. Cavadini, Indirect detection of nitrogen-14 in solid-state NMR spectroscopy, Prog. Nucl. Magn. Reson. Spectrosc., 56 (2010) 46-77.
[29] B.J. van Rossum, H. Forster, H.J.M. de Groot, High-field and high-speed CP-MAS ^{13}C NMR heteronuclear dipolar-correlation spectroscopy of solids with frequency-switched Lee-Goldburg homonuclear decoupling, J. Magn. Reson., 124 (1997) 516-519.
[30] B. Langer, L. Schnell, H.W. Spiess, A.R. Grimmer, Temperature calibration under ultrafast MAS conditions, J. Magn. Reson., 138 (1999) 182-186.
[31] S. Hayashi, K. Hayamizu, Chemical-shift standards in high-resolution solid-state NMR (1): ^{13}C, ^{29}Si and ^{1}H nuclei, Bull. Chem. Soc. Jpn., 64 (1991) 685-687.
[32] I. Schnell, A. Lupulescu, S. Hafner, D.E. Demco, H.W. Spiess, Resolution enhancement in multiple-quantum MAS NMR spectroscopy, J. Magn. Reson., 133 (1998) 61-69.
[33] W. Sommer, J. Gottwald, D.E. Demco, H.W. Spiess, Dipolar heteronuclear multiple-quantum NMR-spectroscopy in rotating solids, J. Magn. Reson., Ser. A, 113 (1995) 131-134.
[34] Z.H. Gan, J.P. Amoureux, J. Trebosc, Proton-detected ^{14}N MAS NMR using homonuclear decoupled rotary resonance, Chem. Phys. Lett., 435 (2007) 163-169.
[35] T.G. Oas, R.G. Griffin, M.H. Levitt, Rotary resonance recoupling of dipolar interactions in solid-state Nuclear Magnetic-Resonance spectroscopy, J. Chem. Phys., 89 (1988) 692-695.
[36] A.L. Webber, S. Masiero, S. Pieraccini, J.C. Burey, A.S. Tatton, D. Iuga, T.N. Pham, G.P. Spada, S.P. Brown, Identifying Guanosine Self Assembly at Natural Isotopic Abundance by High-Resolution ^{1}H and ^{13}C Solid-State NMR Spectroscopy, J. Am. Chem. Soc., 133 (2011) 19777-19795.
[37] A.E. Bennett, C.M. Rienstra, M. Auger, K.V. Lakshmi, R.G. Griffin, Heteronuclear decoupling in rotating solids, J. Chem. Phys., 103 (1995) 6951-6958.
[38] I. Scholz, P. Hodgkinson, B.H. Meier, M. Ernst, Understanding two-pulse phase-modulated decoupling in solid-state NMR, J. Chem. Phys., 130 (2009) 114510.
[39] G. Metz, X.L. Wu, S.O. Smith, Ramped-amplitude cross-polarization in magic-angle-spinning NMR, J. Magn. Reson., Ser. A, 110 (1994) 219-227.
[40] C.R. Morcombe, K.W. Zilm, Chemical shift referencing in MAS solid state NMR, J. Magn. Reson., 162 (2003) 479-486.
[41] S. Hayashi, K. Hayamizu, Chemical-shift standards in high-resolution solid-state NMR (2): ^{15}N nuclei, Bull. Chem. Soc. Jpn., 64 (1991) 688-690.
[42] R.K. Harris, E.D. Becker, S.M.C. De Menezes, P. Granger, R.E. Hoffman, K.W. Zilm, Further conventions for NMR shielding and chemical shifts (IUPAC recommendations 2008), Pure and Applied Chemistry, 80 (2008) 59-84.
[43] G.E. Martin, C.E. Hadden, Long-range ^{1}H-^{15}N heteronuclear shift correlation at natural abundance, Journal of Natural Products, 63 (2000) 543-585.
[44] A. Bielecki, A.C. Kolbert, M.H. Levitt, Frequency-switched pulse sequences - homonuclear decoupling and dilute spin nmr in solids, Chem. Phys. Lett., 155 (1989) 341-346.
[45] M.H. Levitt, A.C. Kolbert, A. Bielecki, D.J. Ruben, High-resolution ^{1}H-NMR in solids with frequency-switched multiple-pulse sequences, Solid State Nucl. Magn. Reson., 2 (1993) 151-163.
[46] B.M. Fung, A.K. Khitrin, K. Ermolaev, An improved broadband decoupling sequence for liquid crystals and solids, J. Magn. Reson., 142 (2000) 97-101.
[47] S.J. Clark, M.D. Segall, C.J. Pickard, P.J. Hasnip, M.J. Probert, K. Refson, M.C. Payne, First principles methods using CASTEP, Z. Kristallogr., 220 (2005) 567-570.
[48] C.J. Pickard, F. Mauri, All-electron magnetic response with pseudopotentials: NMR chemical shifts, Phys. Rev. B: Condens. Matter, 63 (2001) 245101.
[49] J.R. Yates, C.J. Pickard, F. Mauri, Calculation of NMR chemical shifts for extended systems using ultrasoft pseudopotentials, Phys. Rev. B: Condens. Matter, 76 (2007) 024401.

[50] J.P. Perdew, K. Burke, M. Ernzerhof, Generalized gradient approximation made simple, Phys. Rev. Lett., 77 (1996) 3865-3868.
[51] A. Tkatchenko, M. Scheffler, Accurate molecular Van der Waals interactions from ground-state electron density and free-atom reference data, Phys. Rev. Lett., 102 (2009) 073005.
[52] D. Vanderbilt, Soft self-consistent pseudopotentials in a generalized eigenvalue formalism, Phys. Rev. B: Condens. Matter, 41 (1990) 7892-7895.
[53] S. Sturniolo, T.F.G. Green, R.M. Hanson, M. Zilka, K. Refson, P. Hodgkinson, S.P. Brown, J.R. Yates, Visualization and processing of computed solid-state NMR parameters: MagresView and MagresPython, Solid State Nucl. Magn. Reson., 78 (2016) 64-70.
[54] G.N.M. Reddy, D.S. Cook, D. Iuga, R.I. Walton, A. Marsh, S.P. Brown, An NMR crystallography study of the hemihydrate of 2 ', 3 '-O-isopropylidineguanosine, Solid State Nucl. Magn. Reson., 65 (2015) 41-48.
[55] A.L. Webber, L. Emsley, R.M. Claramunt, S.P. Brown, NMR crystallography of campho 2,3-c pyrazole (Z '=6): Combining high-resolution ^{1}H-^{13}C solid-state MAS NMR spectroscopy and GIPAW chemical-shift calculations, J. Phys. Chem. A, 114 (2010) 10435-10442.
[56] B. Elena, A. Lesage, S. Steuernagel, A. Bockmann, L. Emsley, Proton to carbon-13 INEPT in solid-state NMR spectroscopy, J. Am. Chem. Soc., 127 (2005) 17296-17302.
[57] M. Bak, J.T. Rasmussen, N.C. Nielsen, SIMPSON: A general simulation program for solid-state NMR spectroscopy, J. Magn. Reson., 147 (2000) 296-330.
[58] A.L. Webber, B. Elena, J.M. Griffin, J.R. Yates, T.N. Pham, F. Mauri, C.J. Pickard, A.M. Gil, R. Stein, A. Lesage, L. Emsley, S.P. Brown, Complete ^{1}H resonance assignment of beta-maltose from ^{1}H-^{1}H DQ-SQ CRAMPS and ^{1}H(DQ-DUMBO)-^{13}C SQ refocused INEPT 2D solid-state NMR spectra and first principles GIPAW calculations, Phys. Chem. Chem. Phys., 12 (2010) 6970-6983.